Supplementary data

Nitrophenylfurfural grafted amino functionalized silica nanoparticles for adsorptive removal of tartazine dye from water

Syed Salman Shafqat[1]*, Bushra Zafar[2], Syeda Amna Masood[3], Syed Rizwan Shafqat[4], Hafeez Ullah Khan[3], Asad Syed[5], Ali H. Bahkali[5], Sadaf Mutahir[6], Muhammad Asim Khan[6], Guobao Xu[7,8], Muhammad Nadeem Zafar[8,9]*

[1]Department of Chemistry, Division of Science and Technology, University of Education, Lahore 54770, Pakistan
[2]Department of Chemistry and Forensics, Nottingham Trent University, Nottingham NG11 8NS, UK
[3]Department of Pharmaceutics, College of Pharmacy, University of Sargodha, Sargodha 40100, Pakistan
[4]Department of Chemistry, University of Sialkot, Sialkot 51300, Pakistan
[5]Department of Botany and Microbiology, College of Science, King Saud University, PO Box 2455, Riyadh 11451, Saudi Arabia
[6]School of Chemistry and Chemical Engineering, Linyi University, Linyi 276005, China
[7]School of Applied Chemistry and Engineering, University of Science and Technology of China, No. 96 Jinzhai Road, Hefei, Anhui, 230026, People's Republic of China
[8]State Key Laboratory of Electroanalytical Chemistry, Changchun Institute of Applied Chemistry, Chinese Academy of Sciences, 5625 Renmin Street, Changchun, 130022, People's Republic of China
[9]Department of Chemistry, University of Gujrat, Gujrat 50700, Pakistan

***Corresponding author emails:** salman.shafqat@ue.edu.pk (S.S. Shafqat) and znadeempk@gmail.com, nadeem.zafar@uog.edu.pk; ORCID ID: 0000-0002-2109-7601 (M.N. Zafar)

Section S1

The quantity of TTZ adsorbed onto NPF-SiNPs was calculated using the equation S1 as follows:

$$q = \frac{[TTZ]_i - [TTZ]_e}{m} \times V \tag{S1}$$

The TTZ removal efficiency was calculated using the equation S2 as follows:

$$TTZ\ removal, \% = \frac{[TTZ\}_i - [TTZ\}_e}{[TTZ]_i} \times 100 \tag{S2}$$

where q is TTZ adsorption capacity (mg/g), $[TTZ]_i$ is initial TTZ concentration (mg/L), $[TTZ]_e$ is equilibrium TTZ concentration (mg/L), V is the volume of TTZ solution (L), and m is the mass of NPF-SiNPs (g).

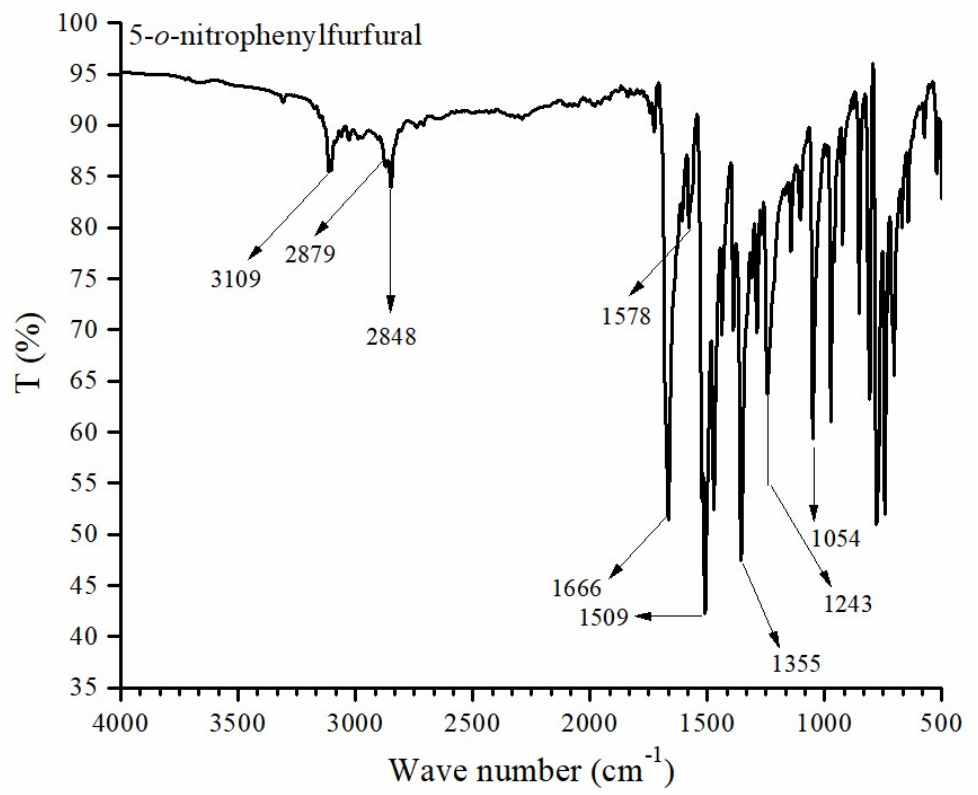

Figure S1. FTIR spectrum of *o*-nitrophenylfurfural

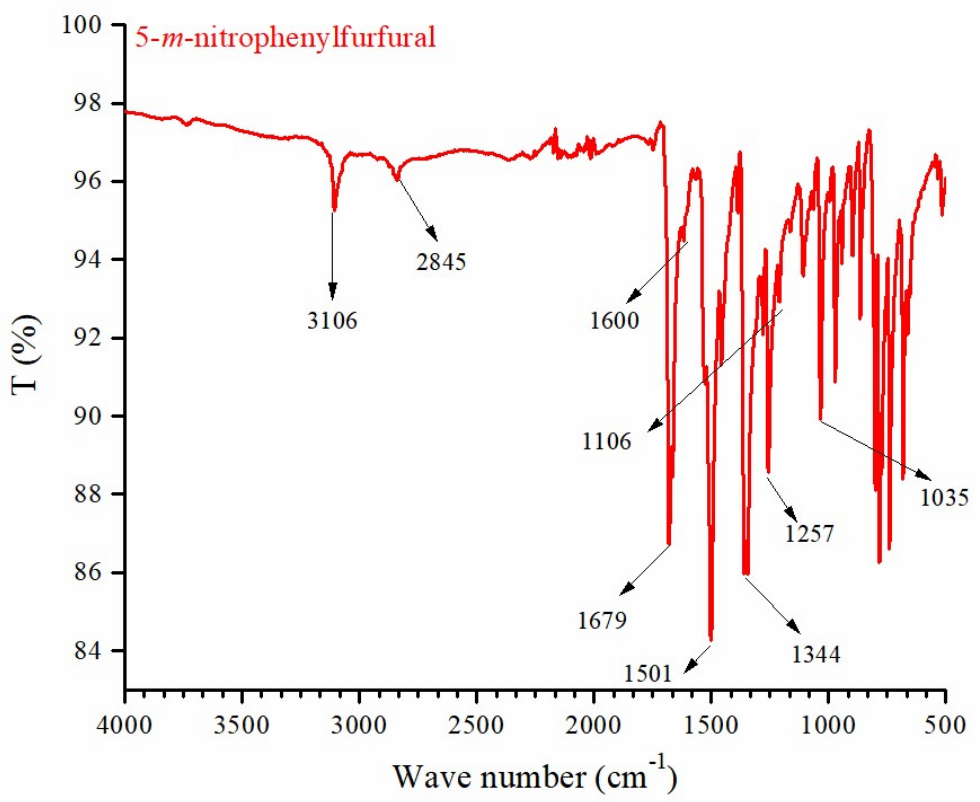

Figure S2. FTIR spectrum of *m*-nitrophenylfurfural

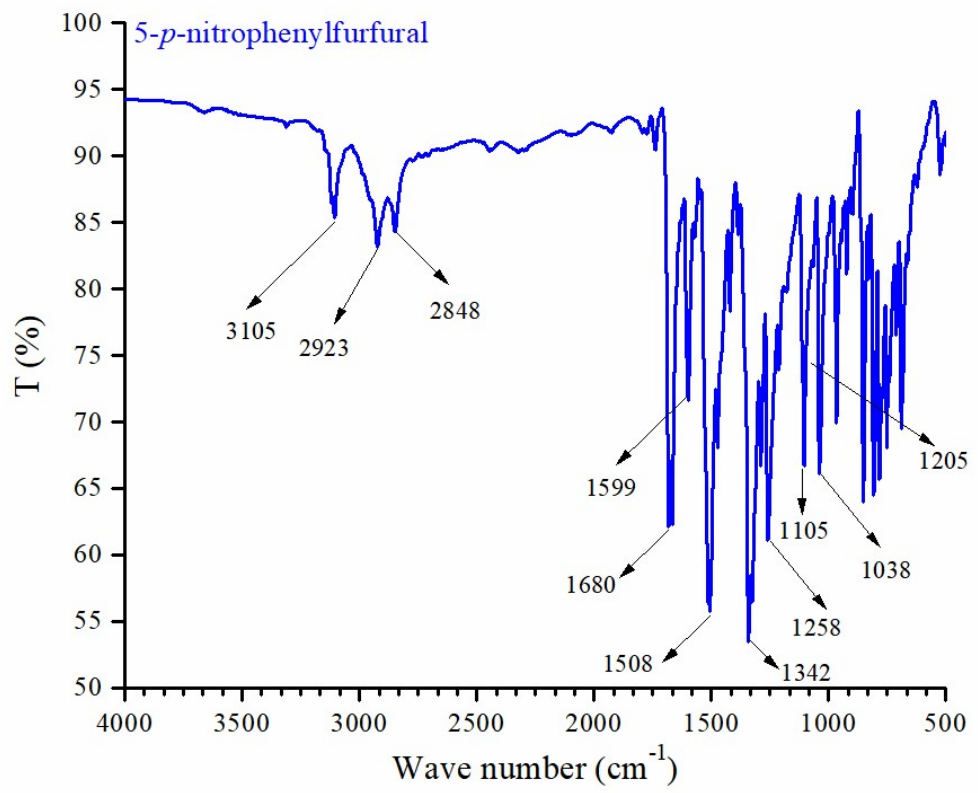

Figure S3. FTIR spectrum of *p*-nitrophenylfurfural

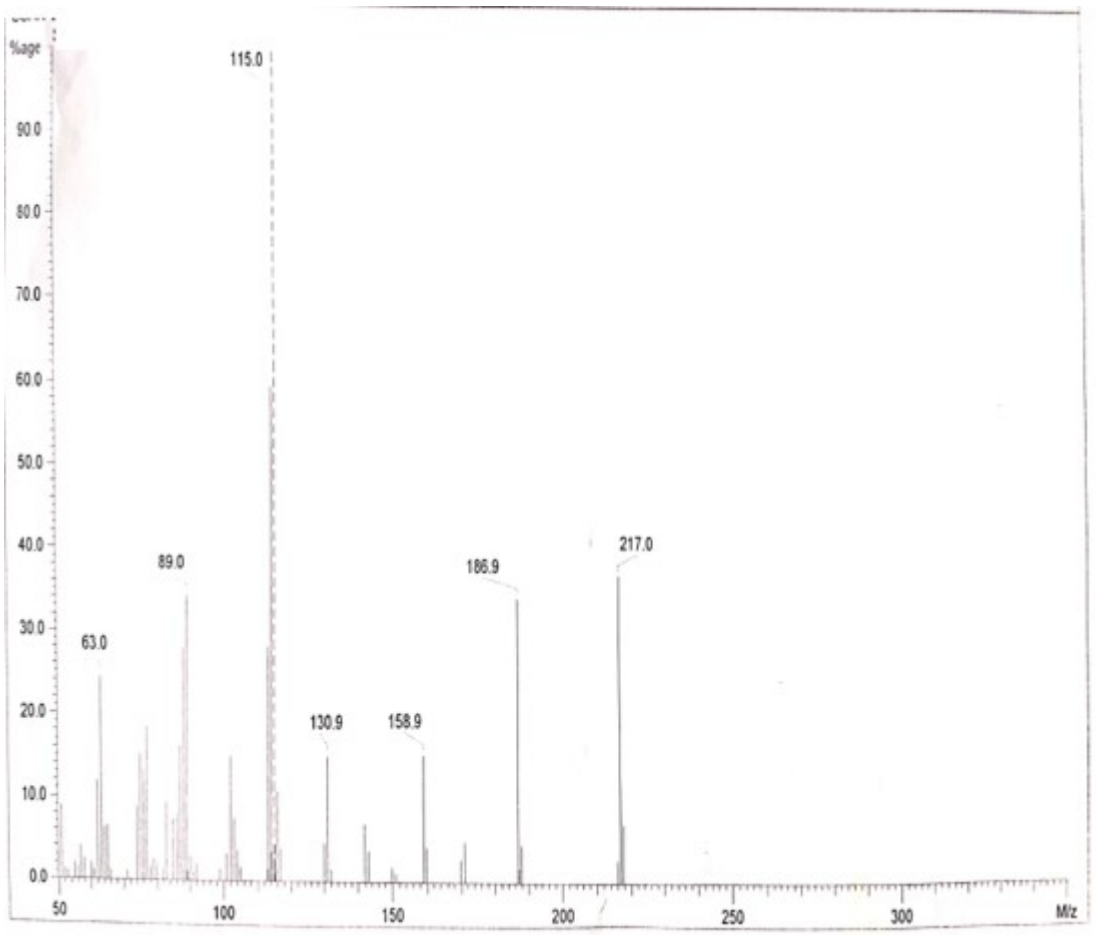

Figure S4. Mass fragmentation pattern of 5-*o*-nitrophenylfurfural

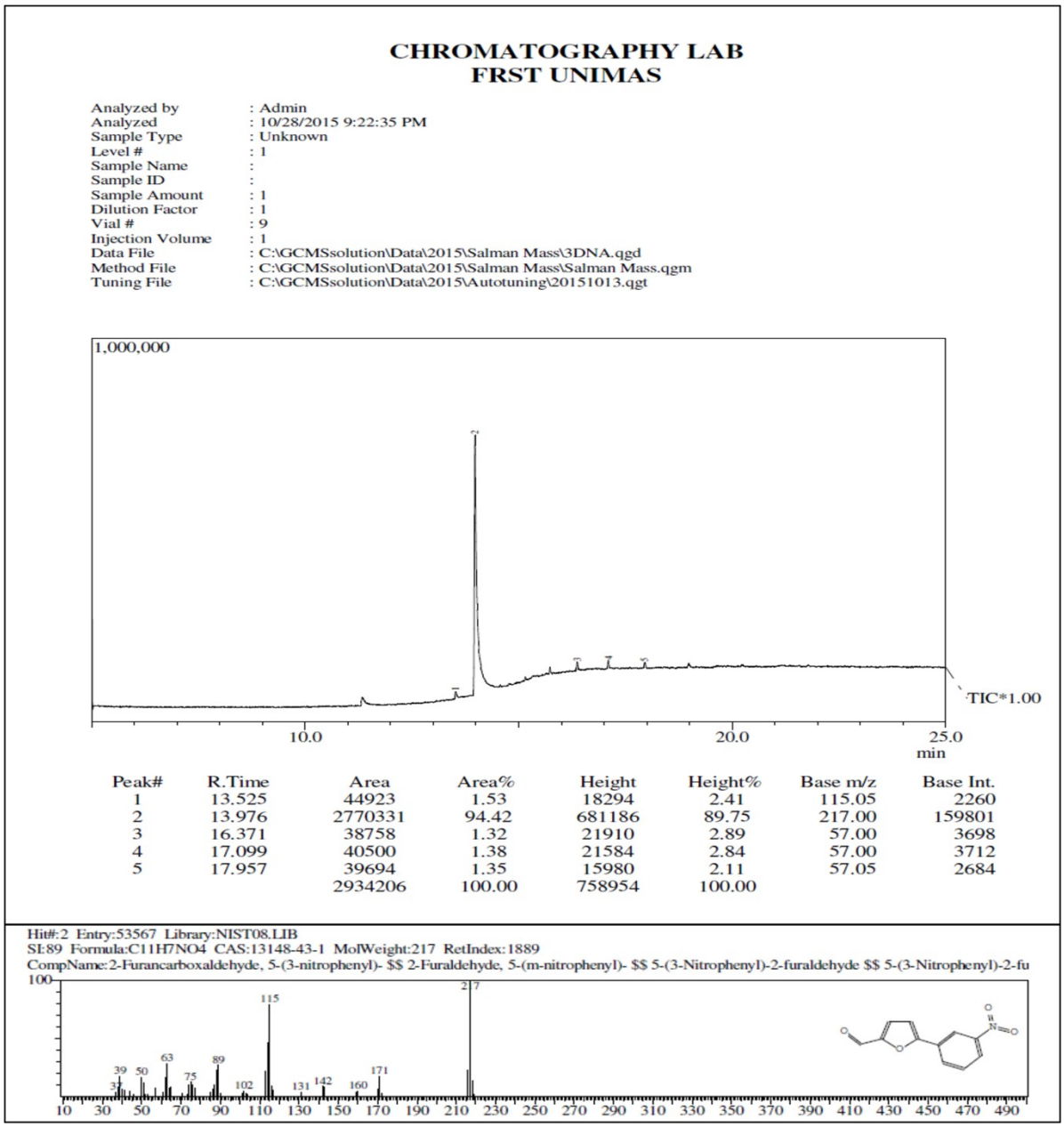

Figure S5. GC and mass fragmentation pattern of 5-*m*-nitrophenylfurfural

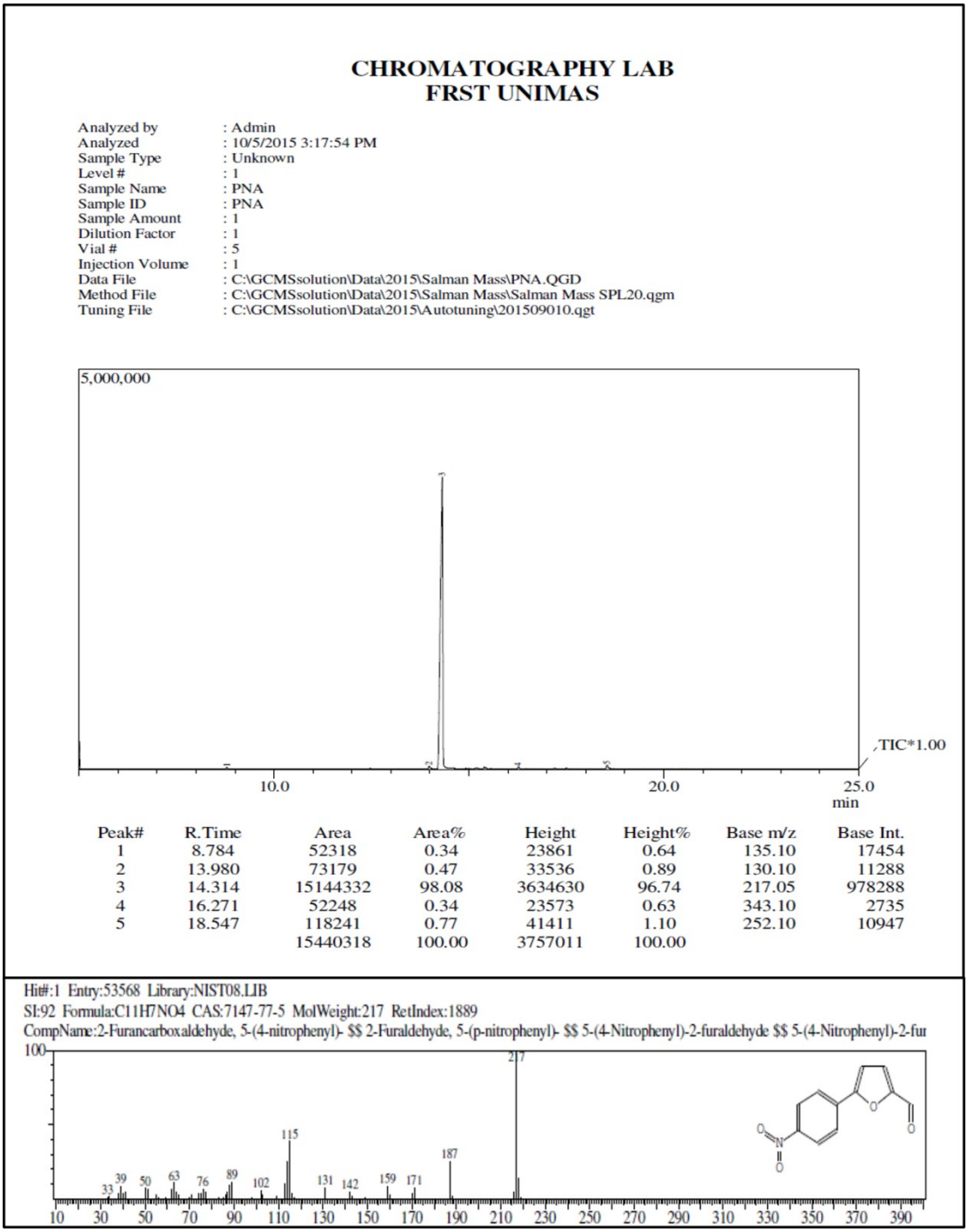

Figure S6. GC and mass fragmentation pattern of 5-*p*-nitrophenylfurfural

Table S1. Characteristics of nitrophenylfurfural

Product	**Yield**	**MP (K)**	**IR (cm^{-1})**	**Mass**
p-Nitrophenylfurfural	42	477	3100 (Ar C-H), 2880, 2830(C-H), 1675 (C=O), 1580, 1519,1325 (N-O), 1240, 1200, 1145,1054 (C-N, C-O, C-H)	217 (100%) M^+
o-Nitrophenylfurfural	49	364	3109 (Ar C-H), 2879, 2848(C-H), 1666 (C=O), 1578, 1509,1355 (N-O), 1243, 1205, 1144,1054 (C-N, C-O, C-H)	217 (100%) M^+
m-Nitrophenylfurfural	45	418	3120 (Ar C-H), 2879, 2828(C-H), 1670 (C=O), 1578, 1501,1345 (N-O), 1240, 1215, 1140,1054 (C-N, C-O, C-H)	217 (100%) M^+

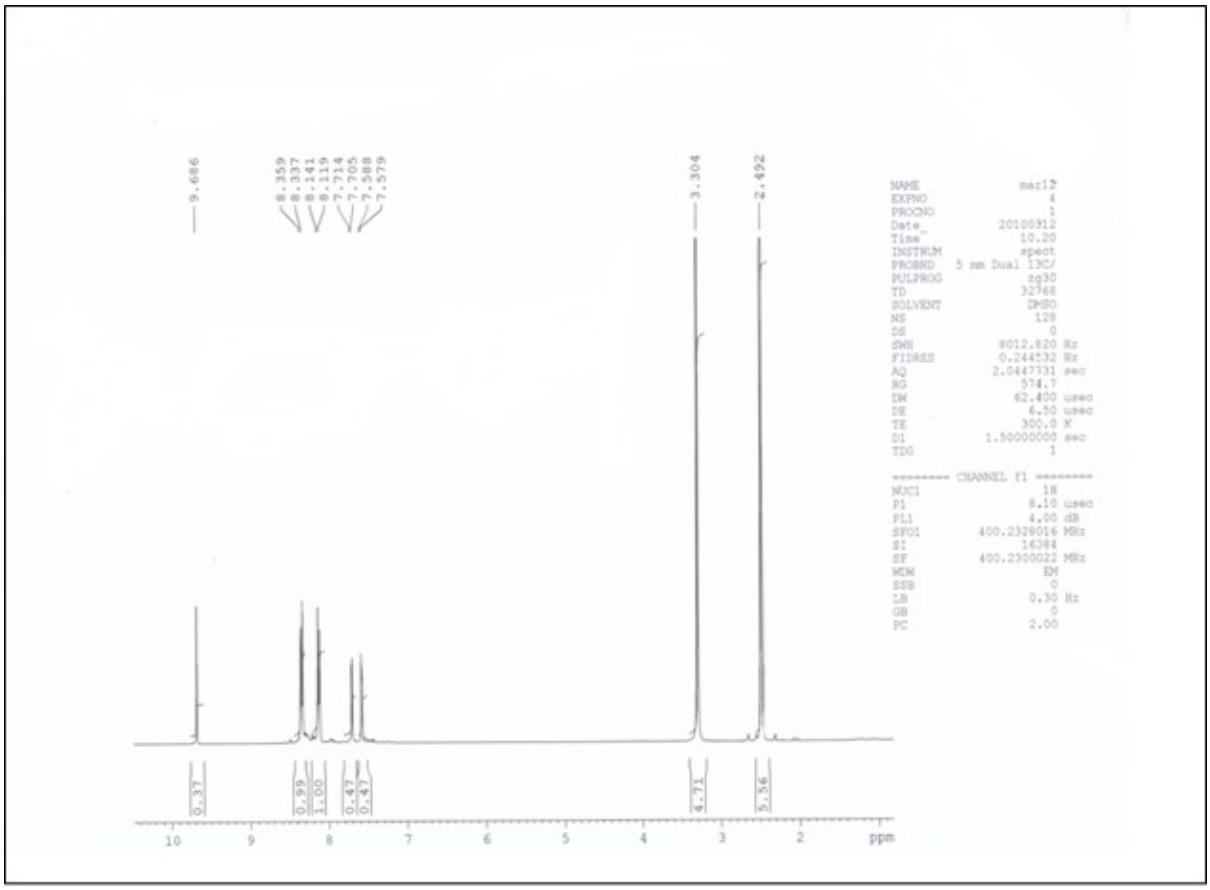

Figure S7. NMR spectrum of 5-*p*-nitrophenylfurfural

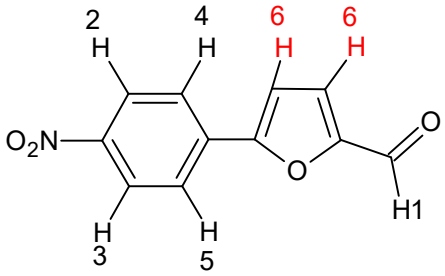

Figure S8. H-environment of 5-*p*-nitrophenylfurfural

Section S2

There was a total of six types of H-atoms present in the molecule as presented in Figure S8. All these protons are labelled in the following molecular structure.

^{1}H-NMR: (DMSO, 400 MHz) δ: 9.68 (1H, S, COH), 8.33 (1H, dd, J = 8.8 and 3.5 Hz, H-7), 8.35 (1H, dd, J = 8.8 and 3.0 Hz, H-9), 8.11 (1H, dd, J = 8.8 and 1.8 H_2, H-6), 8.14 (1H, dd, J = 8.2, and 2.5 Hz, H-10), 7.58 (2H, d, J = 8.5 Hz, H-3 and H-2).

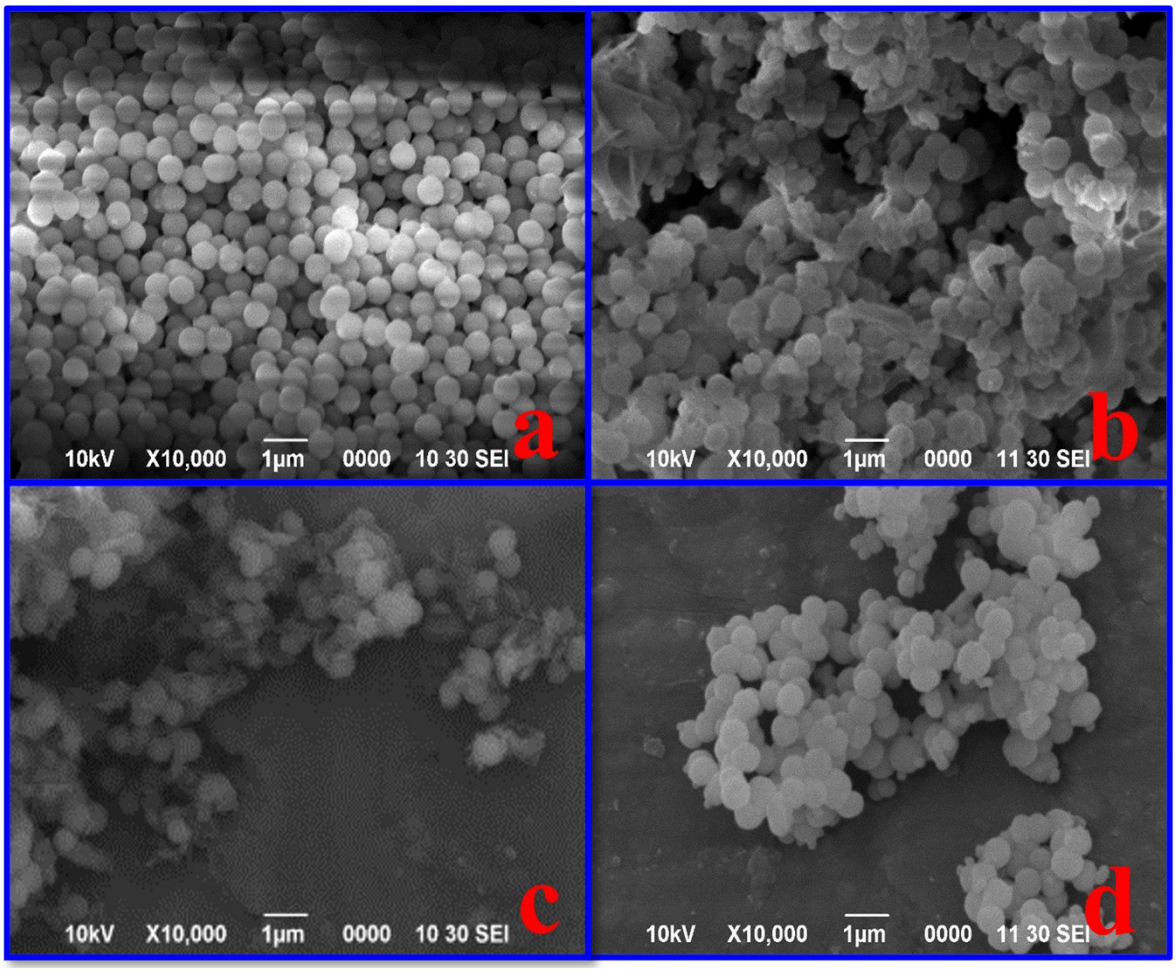

Figure S9. SEM images of (a) AFSi-NPs, (b) *o*-NPF-SiNPs, (c) *m*-NPF-SiNPs, (d) *p*-NPF-SiNPs

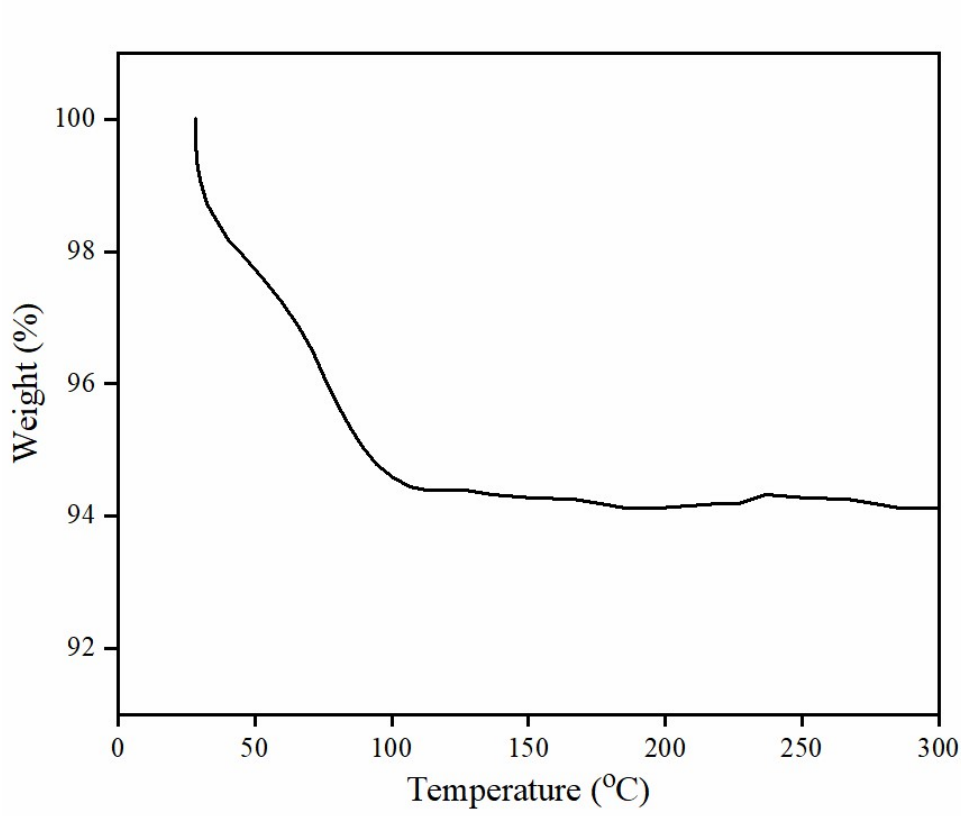

Figure S10. TGA curves of p-SiNPs

Table S2. Thermal characterization (TGA) of AFSi-NPs and NPF-SiNPs

Sample	Decomposition steps	Temperature range (°C)	Weight loss (wt%)	Major species evolved
AFSi-NPs	1	30-120	2	H_2O, CO_2
	2	125-380	4	H_2O, CO_2
	3	381-700	9.6	CO_2, H_2O, NH3, CH2, CH4, N2H4
p-NPF-SiNPs	1	30-89	2	H_2O, CO_2
	2	90-168	5	H_2O, CO_2, NO_x
	3	169-372	6	$C_5H_{10}O$, R-O-R,
	4	373-480		CH_3COCH_3,
	5	481-700	9	CH_4, C_2H_6,
				NO_X, N_2H_4,
o-NPF-SiNPs	1	28-100	2	H_2O, CO_2
	2	101-250	6.	H_2O, CO_2, NO_x
	3	251-434	6.8	$C_5H_{10}O$, R-O-R,
				CH_3COCH3,
	4	437-700	8	CH4, C_2H_6,
				NOX, N_2H_4,
m-NPF-SiNPs	1	28-120	4	H_2O, CO_2
	2	121-275	5	H_2O, CO_2, NO_x
	3	276-446	7	C5H10O, R-O-R,
	4	447-700	9	CH_3COCH_3,
				CH_4, C_2H_6,
				NO_X, N_2H_4,

Table S3. Elemental contents of AFSi-NPs and NPF-SiNPs

Sample	**Weight**	**Elements**			**Simplest empirical formula**		
		Carbon	Hydrogen	Nitrogen	Carbon	Hydrogen	Nitrogen
AFSi-NPs	1.766	3.540	2.13	0.42	1	7.170	1
p-NPF-SiNPs	1.732	33.43	3.05	6.13	6.360	6.914	1
o-NPF-SiNPs	1.711	48.58	2.84	5.42	10.45	7.281	1
m-NPF-SiNPs	1.730	22.86	4.44	3.15	8.463	19.59	1

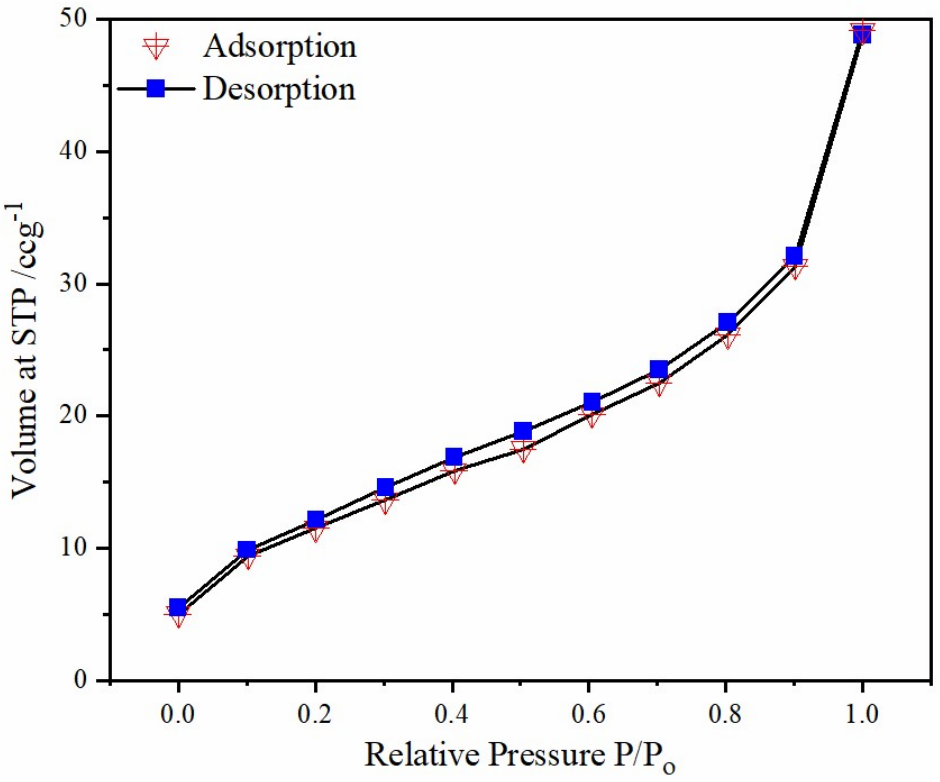

Figure S11. Adsorption/desorption isotherms of p-SiNPs

Table S4. BET study of NPF-SiNPs

Sample	**Specific surface area (m^2/g)**	**Pore volume (cm^3/g)**	**Pore diameter (nm)**
p-NPF-SiNPs	80	0.721	18
o-NPF-SiNps	47		
m-NPF-SiNPs	21		

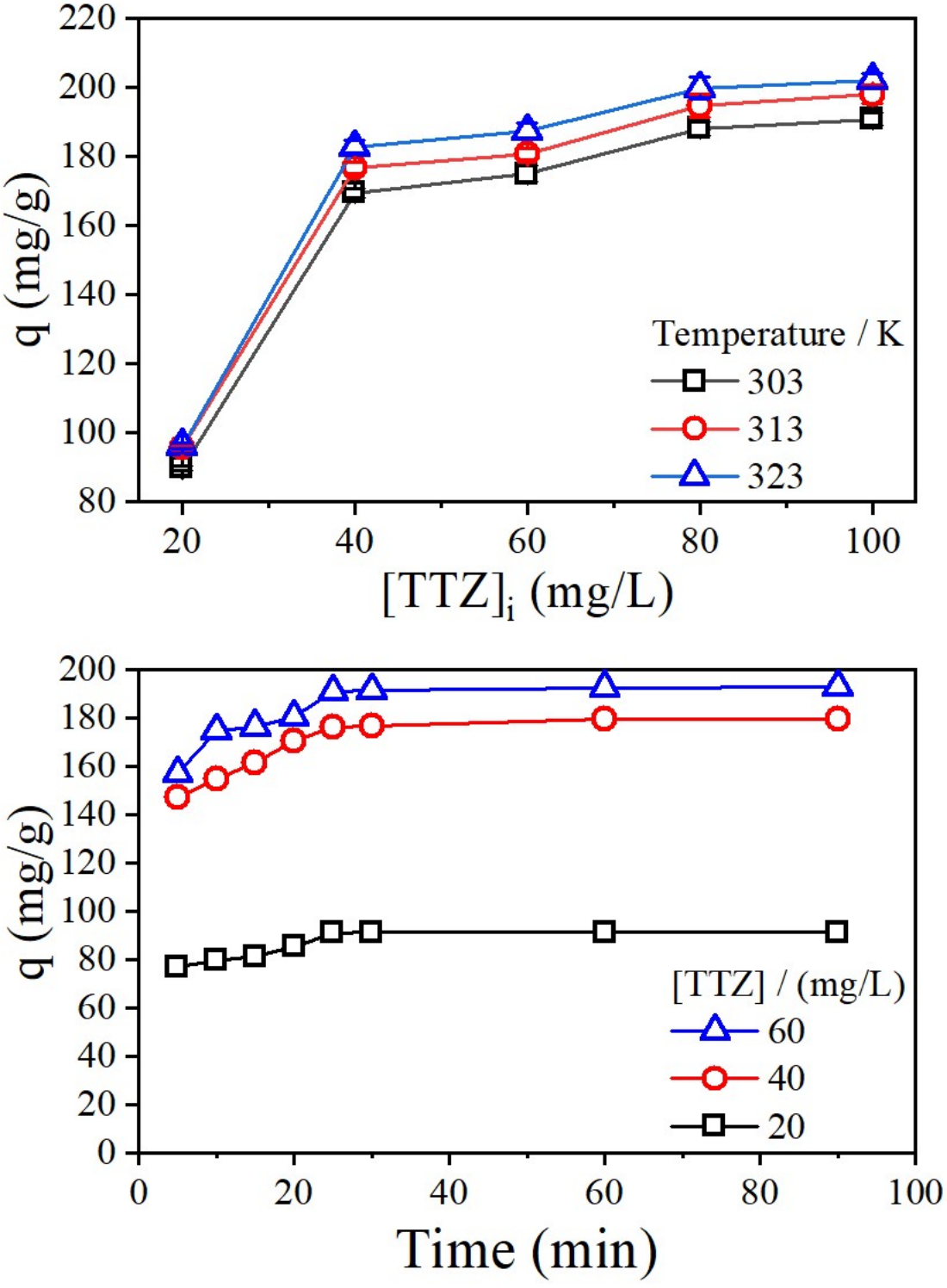

Figure S12. Effect of initial TTZ concentrations (under 303-323 K) and time (for 20-60 mg/L TTZ) on adsorption of TTZ onto *p*-NPF-SiNPs

Section S3. Adsorption isotherm models

Langmuir adsorption model explains the monolayer coverage of TTZ molecules onto *p*-NPF-SiNPs surface leading to homogenous adsorption over the adsorbent surface and Freundlich model explains the multilayer coverage of adsorbent sites by adsorbate, leading to heterogeneous adsorption on the surface of the adsorbent. The following equations S3 and S4 show the non-linear relationship of Langmuir, and Freundlich, respectively [1-3].

$$q = \frac{Q_{th}\, b_L C_e}{1 + b_L C_e} \quad \text{(S3)}$$

$$q = K_F C_e^{1/n} \quad \text{(S4)}$$

Where, Q_{th} (mg/g): maximum monolayer Langmuir adsorption capacity of TTZ onto *p*-NPF-SiNPs, b_L (L/mg): Langmuir constant (related to affinity of adsorption energy and binding sites), K_F ((mg/g)(mg/L)$^{1/n}$): Freundlich constant, n: adsorption intensity.

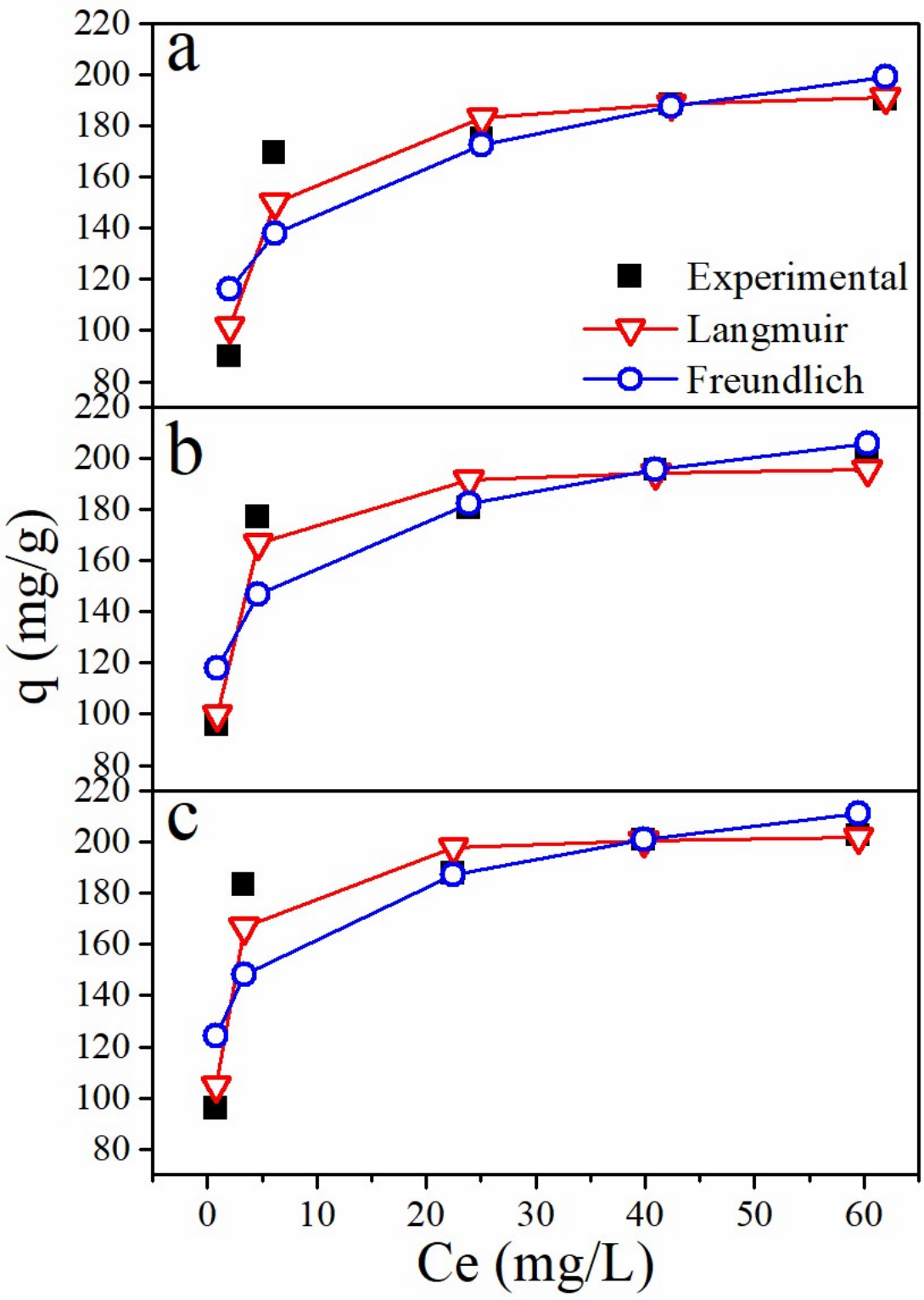

Figure S13. Application of Langmuir, and Freundlich models for TTZ adsorption onto *p*-NPF-SiNPs at (a) 303, (b) 313 and (c) 323K

Section S4. Kinetics models

The linear forms of pseudo-first (PF)-order and pseudo-second (PS)-order are shown by equation S5 and S6 respectively [4, 5].

$$\log\ (q - q_{t1}) = \log q - \frac{K_1 t}{2.303} \quad \text{(S5)}$$

$$\frac{t}{q_{t2}} = \frac{1}{K_2 q^2} + \frac{t}{q} \quad \text{(S6)}$$

where K_1 and K_2 are the adsorption rate constants of PF-order and PS-order kinetic models, in 1/min and g/(mg min), respectively, q and q_{t1} (PF-order), q_{t2} (PS-order) in mg/g, are the equilibrium adsorption uptake (at time t = ∞) and the adsorption uptake (at time t), respectively.

The equation to represent intraparticle diffusion (ID)-model [6] is shown as follows (equation S7).

$$q_t = K_i t^{\frac{1}{2}} + C \quad \text{(S7)}$$

where K_i is the ID-model rate constant in mg/(g $min^{1/2}$) and C is the intercept.

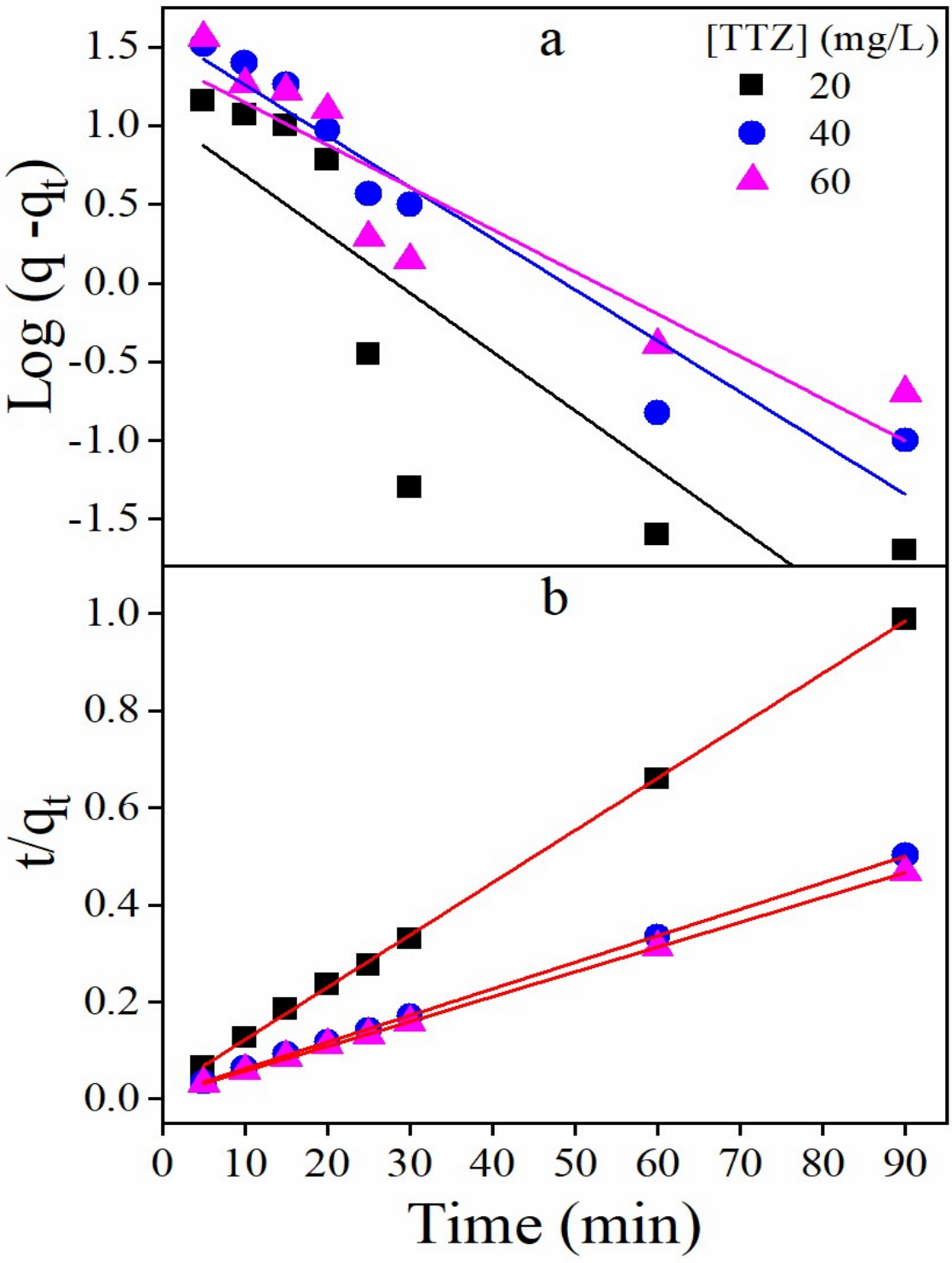
a
[TTZ] (mg/L)
20
40
60
Log (q -q$_t$)
1.5
1.0
0.5
0.0
-0.5
-1.0
-1.5
b
t/q$_t$
1.0
0.8
0.6
0.4
0.2
0.0
0
10
20
30
40
50
60
70
80
90
Time (min)

Figure S14. Application of PF-order (a) and PS-order (b) models on TTZ adsorption using onto *p*-NPF-SiNPs

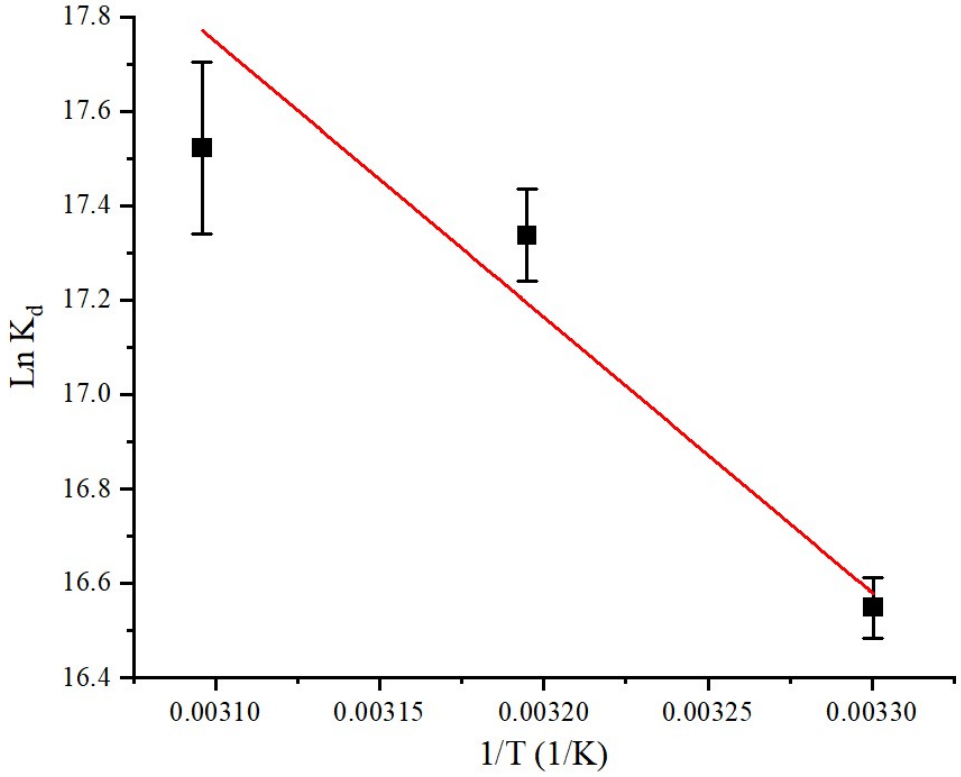

Figure S15. A plot between Ln Kd and 1/T for TTZ adsorption onto onto *p*-NPF-SiNPs

Section S5. Thermodynamic models

Thermodynamic parameters were calculated from the following equations S8 and S9.

$$\Delta G^{o} = -RT \ln K_{d} \quad \text{(S8)}$$

$$\ln K_{d} = -\frac{\Delta H}{RT} + \frac{\Delta S}{R} \quad \text{(S9)}$$

where K_d is the thermodynamic equilibrium constant.

Table S5. Comparison of adsorption capacity of *p*-NPF-SiNPs with other reported adsorbents

Adsorbent	**Adsorption capacity (mg/g)**	**References**
Modified coconut (MCC)	18.41	[7]
Starch-magnesium/aluminum layered double hydroxide (S-Mg/Al LDH)	186.0	[8]
Triethylenetetramine biochar (NCB-TA-PC)	85.47	[9]
RCTLW gelatin beads	263.1	[10]
Modified biomaterial from wheat residues	13.25	[11]
HDTMA-Br-modified Colombian bentonite	40.79	[12]
PS-DVB/Fe_3O_4 nanocomposite	480.0	[13]
Cassava sievate biomass	20.83	[14]
Octadecyltrimethylammonium bromide-modified bentonite (4CEC-NaB)	201.0	[15]
Chitosan-PANI composite	584.0	[16]
Polypyrrole coated tenorite nanoparticles (PPy@TN)	42.50	[17]
Carbon nanotubes modified with silver nanoparticles (5 Ag/CNT)	80.40	[18]
Functionalized multiwall carbon nanotubes (O-MWCNTs)	158.7	[19]
$MgMn_2O_4/Mn_2O_3/Mg_6MnO_8$ (G900)	395.3	[20]
Activated saw dust (ASD)	127.7	[21]
ZnS/CuO/carbon nanotube	183.5	[22]
p-NPF-SiNPs	203.5	Present study

References

1. Langmuir, I., *Adsorption of gases on plane surfaces of glass, mica and platinum.* Journal of the American Chemical Society, 1918. **40**: p. 1361-1403.
2. Freundlich, H., *Adsorption in solutions.* Journal of Physical Chemistry, 1906. **57**: p. 384-410.
3. Temkin, M.J. and V. Pyzhev, *Recent modifications to Langmuir isotherms.* Acta Physiochimica USSR, 1940. **12**: p. 217-222.
4. Ho, Y.-S. and G. McKay, *Pseudo-second order model for sorption processes.* Process Biochemistry, 1999. **34**(5): p. 451-465.
5. Lagergren, S., *About the theory of so-called adsorption of soluble substances.* Kungliga Svenska Vetenskapsakad Handlngar, 1898. **24**(4): p. 1-39.
6. Weber, W.J. and J.C. Jr Morris, *Kinetics of adsorption on carbon from solution.* Journal of the Sanitary Engineering Division, 1963. **89**(2): p. 31-60.
7. Tejada-Tovar, C., Á. Villabona-Ortíz, and Á.D. Gonzalez-Delgado, *Adsorption of Azo-Anionic Dyes in a Solution Using Modified Coconut (Cocos nucifera) Mesocarp: Kinetic and Equilibrium Study.* Water, 2021. **13**(10): p. Article no. 1382.
8. Grover, A., et al., *Magnesium/aluminum layered double hydroxides intercalated with starch for effective adsorptive removal of anionic dyes.* Journal of Hazardous Materials, 2022. **424**: p. Article no. 127454.
9. Mahmoud, M.E., et al., *Adsorption of negatively charged food tartrazine and sunset yellow dyes onto positively charged triethylenetetramine biochar: Optimization, kinetics and thermodynamic study.* Journal of Molecular Liquids, 2020. **318**: p. Article no. 114297.
10. Rigueto, C.V.T., et al., *Emerging contaminants adsorption by beads from chromium (III) tanned leather waste recovered gelatin.* Journal of Molecular Liquids, 2021. **330**: p. Article no. 115638.
11. Ortega-Toro, R., et al., *Effective adsorption of Tartrazine by modified biomaterial from wheat residues.* Ingeniería y competitividad, 2021. **24**(1): p. Article no. 11139.
12. Otavo-Loaiza, R.A., N.R. Sanabria-González, and G.I. Giraldo-Gómez, *Tartrazine Removal from Aqueous Solution by HDTMA-Br-Modified Colombian Bentonite.* The Scientific World Journal, 2019. **2019**: p. Article no. 2042563.
13. Ali, M.A., et al., *Adsorption of Tartrazine anionic dye by novel fixed bed Core-Shell-polystyrene Divinylbenzene/Magnetite nanocomposite.* Alexandria Engineering Journal, 2022. **61**(2): p. 1335-1352.
14. Chukwuemeka-Okorie, H.O., et al., *Adsorption of tartrazine and sunset yellow anionic dyes onto activated carbon derived from cassava sievate biomass.* Applied Water Science, 2021. **11**(2): p. Article no. 27.
15. Sahnoun, S., et al., *Adsorption of tartrazine from an aqueous solution by octadecyltrimethylammonium bromide-modified bentonite: Kinetics and isotherm modeling.* Comptes Rendus Chimie, 2018. **21**(3-4): p. 391-398.
16. Sahnoun, S. and M. Boutahala, *Adsorption removal of tartrazine by chitosan/polyaniline composite: Kinetics and equilibrium studies.* International Journal of Biological Macromolecules, 2018. **114**: p. 1345-1353.
17. Srivastava, V., et al., *Synthesis and application of polypyrrole coated tenorite nanoparticles (PPy@TN) for the removal of the anionic food dye 'tartrazine' and*

divalent metallic ions viz. Pb(ii), Cd(ii), Zn(ii), Co(ii), Mn(ii) from synthetic wastewater. RSC Advances, 2015. **5**(98): p. 80829-80843.
18. Goscianska, J. and R. Pietrzak, *Removal of tartrazine from aqueous solution by carbon nanotubes decorated with silver nanoparticles.* Catalysis Today, 2015. **249**: p. 259-264.
19. Nait-Merzoug, A., et al., *Tartrazine removal from water using functionalized multiwall carbon nanotubes.* Desalination and Water Treatment, 2017. **67**: p. 397-405.
20. Al-Wasidi, A.S., et al., *Facile synthesis and characterization of magnesium and manganese mixed oxides for the efficient removal of tartrazine dye from aqueous media.* RSC Advances, 2023. **13**(9): p. 5656-5666.
21. Rzig, B., et al., *Adsorption performance of tartrazine dye from wastewater by raw and modified biomaterial: Equilibrium, isotherms, kinetics and regeneration studies.* Biomass Conversion and Biorefinery, 2023: p. DOI: 10.1007/s13399-023-03982-8.
22. Sharifpour, E., et al., *In-situ hydrothermal synthesis of CNT decorated by nano ZnS/CuO for simultaneous removal of acid food dyes from binary water samples.* Scientific Reports, 2022. **12**(1): p. Article no. 12381.